Eur. Phys. J. B **9**, 599–604 (1999)

THE EUROPEAN PHYSICAL JOURNAL B

EDP Sciences

A Raman and dielectric study of ferroelectric $Ba(Ti_{1-x}Zr_x)O_3$ ceramics

R. Farhi[1,a], M. El Marssi[1], A. Simon[2], and J. Ravez[2]

[1] Laboratoire de Physique de la Matière Condensée, Université de Picardie Jules Verne, 33 rue Saint-Leu, 80039 Amiens, France
[2] Institut de Chimie de la Matière Condensée de Bordeaux, CNRS, 87 avenue du Dr. A. Schweitzer, 33608 Pessac, France

Received 25 September 1998

Abstract. Dielectric and Raman scattering experiments were performed on various ceramics with composition $Ba(Ti_{1-x}Zr_x)O_3$. Such lead-free, environmental-friendly materials were shown, from dielectric measurements, to exhibit behaviours extending from conventional to relaxor ferroelectrics on increasing the zirconium concentration. The evolution of the Raman spectra was studied as a function of temperature for various compositions, and the spectroscopic signature of the corresponding phases was determined. In the relaxor state, the variation of the integrated intensity of the Raman lines with temperature showed a plateau at low temperature. This anomaly was also detected as a peak in depolarization current measurements, and attributed to ergodicity breaking which characterizes usual relaxor systems. Raman results hint at locally rhombohedral polar nanoregions resulting from the random fields associated with Zr ions.

PACS. 77.84.-s Dielectric, piezoelectric, ferroelectric and antiferroelectric materials – 77.84.Dy Niobates, titanates, tantalates, PZT ceramics, etc. – 61.43.-j Disordered solids

1 Introduction

Relaxor materials are characterized mainly by a frequency dispersion and broad peaks in the dielectric susceptibility versus temperature variation [1]. This last property is of great interest for applications (dielectric for capacitors, actuators,...). However, it appears most often in lead based perovskite-type compounds, such as lead magnoniobate (PMN), lead tin niobate (PSN), lead indium niobate (PIN), lead scandium tantalate (PST), La-modified lead zirconate titanate (PLZT),... The phase diagrams of some lead-free, environmental-friendly, $BaTiO_3$ based ceramics were reported recently by Ravez and Simon [2]. Homovalent or heterovalent substitutions of barium or titanium ions were shown to give rise to various behaviours, including relaxor properties which may appear for some composition-temperature ranges. One of the simplest compounds investigated in this work was $Ba(Ti_{1-x}Zr_x)O_3$ (referred to as BTZ100x in what follows). It involves the homovalent substitution of titanium ($M_{Ti} = 47.9$; Ti^{4+} ionic radius = 74.5 pm) by zirconium ($M_{Zr} = 91.2$; Zr^{4+} ionic radius = 86 pm), and was previously reported to exhibit relaxor properties for substitution rates higher than about 25% [2].

In addition to dielectric measurements, which remain the most demonstrating experiments for the characterization of relaxor properties, Raman scattering has been shown to be a powerful technique for studying the onset of ferroelectric order in polar disordered systems, and more specifically in perovskite-based materials such as PLZT, KTN or KLT (Nb-modified and Li-modified potassium tantalate respectively). The Raman integrated intensity was demonstrated to be proportional to the autocorrelation function of the quasi-static polarization [3,4].

The aim of this work is to try to understand the behaviour of BTZ ceramics for compositions extending from low zirconium contents (which display ferroelectric-type properties) up to the zirconium solubility limit (slightly below which relaxor characteristics are observed), using electrical measurements and Raman scattering, and to compare it with the behaviour of pure barium titanate (referred to as BT in what follows).

Experimental details will be described in the next section. Section 3 will be devoted to dielectric measurements, from which the phase diagram of BTZ will be derived, and the results of Raman scattering experiments for various compositions will be reported in Section 4. A discussion of the whole set of results will be given in the last section of this article, in connection with the behaviour of pure barium titanate.

2 Experimental details

BTZ ceramics were prepared by solid state synthesis using the following chemical reaction:

$$BaCO_3 + (1-x)\,TiO_2 + x\,ZrO_2 \rightarrow Ba(Ti_{1-x}Zr_x)O_3 + CO_2.$$

[a] e-mail: robert.farhi@sc.u-picardie.fr

A calcination for 15 hours at 1200 °C was followed by a 4-hours sintering at 1400 °C. Both heat treatments were conducted under dry oxygen. X-ray diffraction analyses allowed us to determine the limits of the solid solution domain close to BT, in which mixed compounds keep the perovskite structure in the paraelectric phase. The zirconium range which satisfies this condition extends from $x = 0$ to $x = 0.42$. Prior to dielectric measurements, gold electrodes were deposited on the circular faces of the cylindrical platlets 7 mm in diameter and 1 mm thick. Dielectric measurements were performed under dry helium from 75 to 450 K using a Wayne-Kerr component analyser 6425, in the frequency range 10^2-10^5 Hz.

Raman scattering experiments were done using a Dilor Z24 triple monochromator. The spectral resolution was 3 cm^{-1}. The excitation light was the 514.5 nm line of an argon ion laser. Two types of Raman geometries were used. For low temperature studies (from room temperature to 13 K), the samples were stuck to the cold finger of a closed circuit helium cryostat (Cryogenics; temperature accuracy ± 0.1 K), and the scattering angle was slightly shifted by about 10° from full macro-Raman backscattering in order to reduce stray light. For experiments above room temperature, the laser beam was focused through a microscope (light spot diameter $\sim 2\,\mu$m) onto the sample whose temperature was regulated (± 0.1 K) by a Linkam hot stage device. The laser power at the sample was limited to 50 mW and 5 mW in macro and micro-Raman scattering, respectively. All the spectra reported in this work have been corrected by the Bose-Einstein population factor $n(\omega) + 1$.

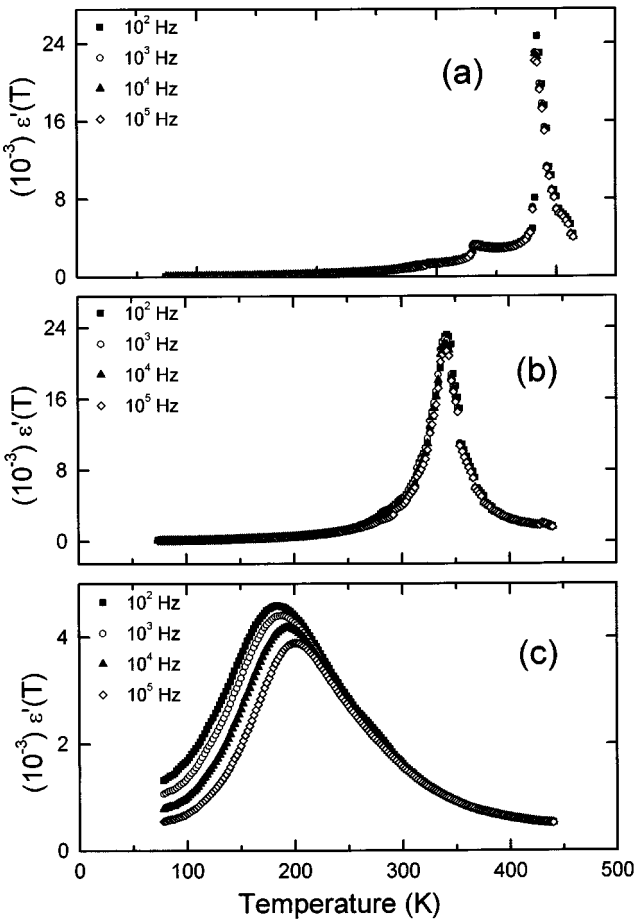

Fig. 1. Real part of the dielectric permittivity of (a) BTZ05, (b) BTZ15 and (c) BTZ40 as a function of the temperature.

3 Dielectric results

The temperature and frequency variations of the real permittivity of BTZ ceramics exhibit three different behaviours, depending upon the substitution rate. For Zr compositions lower than $x \approx 0.10$, the ceramics show conventional ferroelectric properties, with three dielectric anomalies associated with the phase transitions which are known to exist in BT [5], namely cubic to tetragonal at T_c, tetragonal to orthorhombic at T_2, and orthorhombic to rhombohedral at T_1. This behaviour is illustrated in Figure 1a for $x = 0.05$. In the composition range between $x \approx 0.10$ and $x \approx 0.27$, only one transition is observed through a strong and slightly broadened peak in the real part of the dielectric susceptibility (Fig. 1b corresponds to $x = 0.15$), whose temperature does not depend on the frequency. According to Cross [1], such an anomaly should be associated to a "diffuse paraelectric-ferroelectric transition". For Zr- richer compounds, the dielectric peak becomes broader and a frequency dispersion of the permittivity takes place, as reported in Figure 1c for $x = 0.40$. In addition, the temperature T_m of the dielectric maximum is shifted to lower values for decreasing frequencies. This shift obeys a Vogel-Fulcher law with a freezing temperature of 145 ± 15 K. This is known to be one of the characteristics of relaxor systems.

The phase diagram of the BTZ system has been obtained from the anomalies observed in the dielectric susceptibility measurements, and is represented in Figure 2. It is in fairly good agreement with the results previously obtained by Hennings *et al.* [6]. It can be seen that the transition temperatures between phases appearing in BT converge, on increasing the Zr content, to a single point with composition $x \sim 0.10$. Beyond this point, the tetragonal and orthorhombic phases disappear, and the transition line is defined from the frequency- independent maximum of the dielectric susceptibility for the "diffuse transition"-like compositions, or from the maximum at a frequency of 10^3 Hz for the relaxor compounds.

4 Raman scattering

In its high temperature cubic phase, barium titanate has the perovskite cubic structure. Using a standard group theory analysis, normal optic modes can be shown to belong to the $3T_{1u} \oplus T_{2u}$ irreducible representations of the point group O_h. When entering the tetragonal C_{4v} phase, the IR active T_{1u} modes are expected to split into

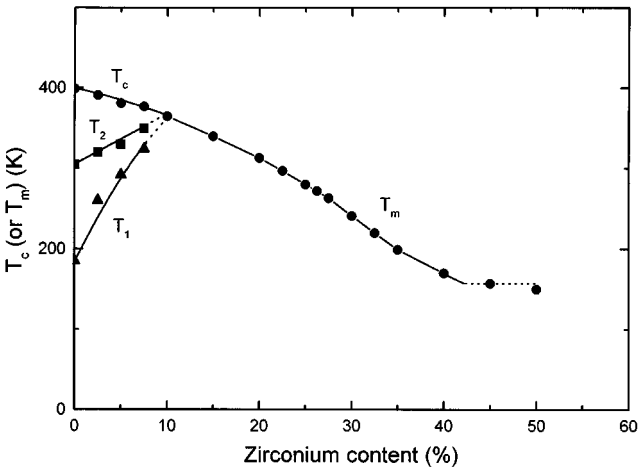

Fig. 2. Phase diagram (composition *vs.* temperature) of the barium titanate-barium zirconate system.

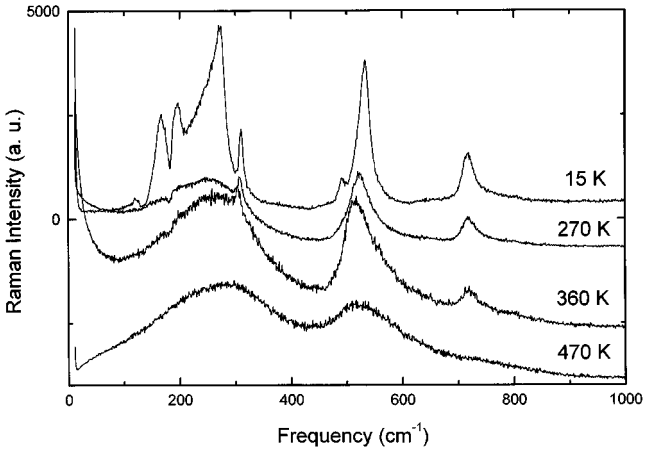

Fig. 3. Depolarized Raman spectra of BTZ05 ($x = 0.05$) in the rhombohedral (15 K and 270 K) tetragonal (360 K) and paraelectric cubic phases (470 K). The intensities have been corrected for the Bose-Einstein factor.

$A_1 \oplus E$, and the silent mode T_{2u} into $B_1 \oplus E$. The cubic-to-tetragonal transition ($T_c \approx 400$ K) in BT is not yet completely understood. The static positions of atoms in the tetragonal phase, calculated from a quasi-harmonic model, are moved to positive and negative z-directions for Ti and O atoms respectively, when referred to the barium ion chosen as the origin [5]. Nevertheless, this purely displacive model cannot account for the complex dynamic behaviour of the transition, observed through an overdamped soft mode which hints at a strong order-disorder component. None of the other modes are involved in the transition, including in the low frequency region [7]. The assignment of the Raman lines is not unambiguous, and a puzzling antiresonance effect at 180 cm^{-1} has been attributed [7] to a coupling between the A_1 transverse optic (TO) phonons.

Because of the ceramic character of BTZ, which gives rise to a strong depolarization of the incident and scattered light, Raman spectra are not expected to be polarized. In addition, because of the random grain orientation in the ceramics, the directions of the phonon wavevectors are randomly distributed with respect to crystallographic axes from one grain to another, and mode mixing together with long range electrostatic force effects should be therefore responsible for a broadening of the lines. The depolarized Raman spectra of BTZ05 are shown in Figure 3 for the rhombohedral (15 K and 270 K) tetragonal (360 K) and paraelectric cubic phases (470 K). Raman spectra recorded in the orthorhombic phase could not be distinguished from those in rhombohedral phase. The cubic paraelectric phase is characterized by two very broad lines centered at about 285 and 520 cm^{-1}, as already reported for pure barium titanate [7]. It should be pointed out that normal modes are not Raman active in the paraelectric phase, and the origin of their activation should be found in a strong disorder already occurring at high temperature. In the tetragonal phase (360 K), and despite the line broadening, most of the features already reported and discussed for $BaTiO_3$ by Scalabrin *et al.* [7] are observed. The overdamped transverse E mode is detected through the increase of the scattered intensity below about 100 cm^{-1}. High frequency A_1 TO modes are also observed as broad lines at 250 and 524 cm^{-1}. The interference effect at 180 cm^{-1}, which has been attributed by these authors to the result of a coupling between a narrow and a broad A_1 TO modes (*i.e.*, a Fano-type effect), is clearly visible. This feature, together with the $B_1 + E$ mode at 307 cm^{-1} and the high frequency longitudinal optic (LO) modes at about 720 cm^{-1}, appears only on entering the tetragonal phase, and can be therefore considered as the signature of the cubic-to-tetragonal phase transition. No drastic evolution of the spectra is detected on further cooling, and at 15 K, *i.e.*, in the rhombohedral phase, most of the lines which were already assigned in the tetragonal phase can be easily detected. The asymmetrical shape of the line extending from 210 to 290 cm^{-1} should be related with the high phonon density of states which prevails in this frequency region [7]. However, an additional feature at 119 cm^{-1} comes out in the rhombohedral phase of BTZ05 on cooling down to 15 K. This line was never reported before in BT, but previously detected from IR measurements in barium zirconate [8]. According to the mass ratio Zr/Ti (= 1.9), which is not very far from the square of the frequency ratio 180/119 (= 2.3), it could be associated with a normal mode involving Zr ions motion against the oxygen octahedra.

This assertion is supported by the spectra recorded for BTZ15 and reported in Figure 4. In almost the same way as in BTZ05, the (diffuse) transition from the cubic to the low temperature phase is reflected through the appearance of the high frequency (719 cm^{-1}) LO line and the interference feature at 180 cm^{-1}. The previously narrow B_1 line has merged into the broad and asymmetric peak of density of states. The most interesting observation in the 15 K spectrum is that the line previously recorded at 119 cm^{-1} in BTZ05 has now transformed into

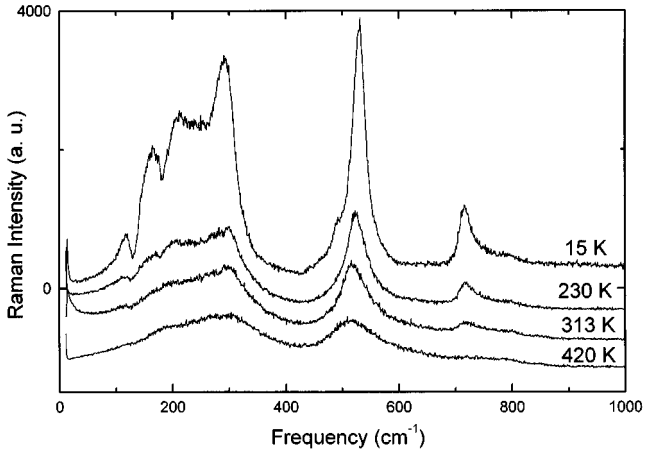

Fig. 4. Depolarized Raman spectra of BTZ15 ($x = 0.15$) in the rhombohedral (15 K, 230 K and 313 K) and in the paraelectric cubic phases (420 K). The intensities have been corrected for the Bose-Einstein factor.

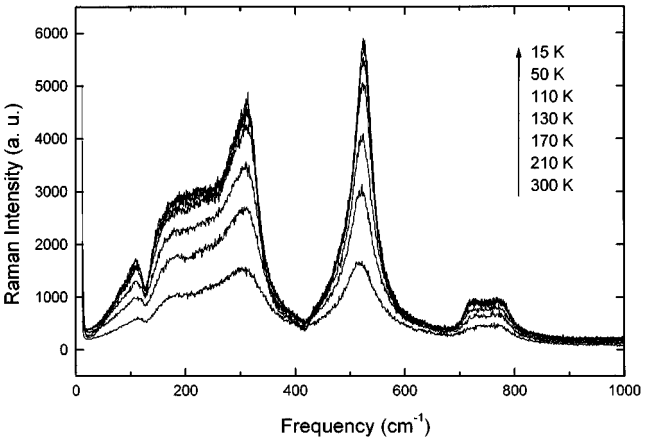

Fig. 6. Depolarized Raman spectra of BTZ40 ($x = 0.40$) at various temperatures between 300 K (bottom spectrum) and 15 K (top spectrum). The intensities have been corrected for the Bose-Einstein factor.

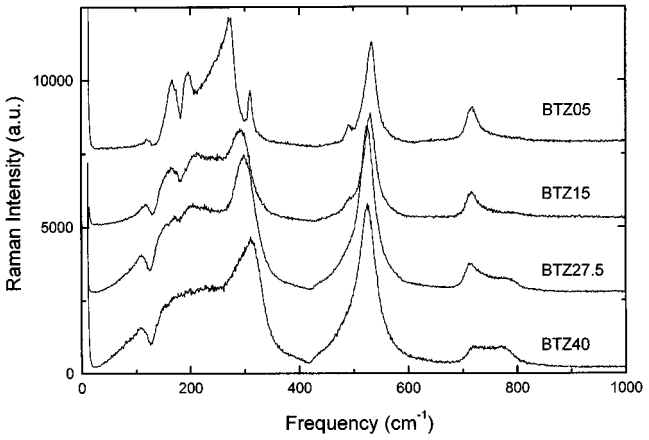

Fig. 5. Raman spectra of BTZ ceramics of compositions $x = 0.05$, 0.15, 0.275 and 0.40 at 15 K.

a dip at 125 cm^{-1}. In addition, there is a strong similarity between the dip at 125 cm^{-1} and the one observed at 180 cm^{-1} in pure BT and in BTZ05. More specifically, the amplitude of the former has increased and is now comparable to that of the latter. This should be correlated with the higher Zr composition, as illustrated in Figure 5 where Raman spectra of BTZ ceramics of compositions $x = 0.05$, 0.15, 0.275 and 0.40 have been compared at 15 K. On increasing x up to 0.40, the interference effect at 125 cm^{-1} becomes stronger, while the one at 180 cm^{-1} progressively fades. In BTZ05, this interference effect does not exist at low temperature because the broadening of the A_1 TO modes, partly associated with the Zr disorder, is less. The coupling between modes [7] is accordingly reduced, and the normal mode involving Zr motion gives rise to a conventional but asymmetric Raman line at 119 cm^{-1}.

Raman spectra for BTZ40 at various temperatures below 300 K are reported in Figure 6. The dip at 125 cm^{-1} persists at temperatures higher than the dielectric susceptibility maximum at ∼180 K. A clear signature of the relaxor phase can be found in the high frequency region, where an extra line appears at ∼780 cm^{-1} in addition to the 720 cm^{-1} LO lines. This extra line is already observed, but with a weaker intensity, in less Zr-rich compounds such as BTZ15 and BTZ27.5 (Fig. 5).

From a Raman point of view, BTZ40 is characterized by a continuous variation of the overall intensity of the spectra with temperature, without any change in width or frequency of the lines, even on crossing the dielectric susceptibility maximum at ∼180 K. This shows that, contrary to what was observed in BTZ05 and, even if less obviously, in BTZ15, no transition exists in BTZ40. This is one of the basic properties of relaxor systems. In order to characterize in a more quantitative way the evolution of the Raman intensity with temperature, we have selected a single line for which the integrated intensity can be easily calculated, namely the TO modes peak at ∼ 520 cm^{-1}. The corresponding data are reported in Figure 7. They show an increase on cooling down to about 120 K. Below this temperature, the integrated Raman intensity exhibits a plateau, in the same way as was previously observed in relaxor 9/65/35 PLZT ceramics [3,9].

5 Discussion

Barium titanate zirconate ceramics are interesting for applications, mainly because these lead-free, environmental-friendly materials exhibit, for some compositions, relaxor properties which are characterized by broad dielectric susceptibility peaks in the room temperature region. This relaxor behaviour is more specifically demonstrated by a frequency dispersion in agreement with Vogel-Fülcher law, as reported in Section 3. These compounds belong to the perovskite family and, in the relaxor phase, their average structure remains cubic down to low temperature,

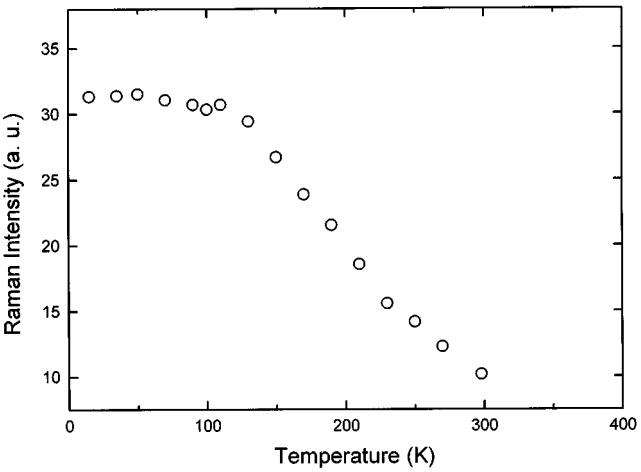

Fig. 7. Raman integrated intensity of the TO high frequency line as a function of the temperature. The intensities have been corrected for the Bose-Einstein factor.

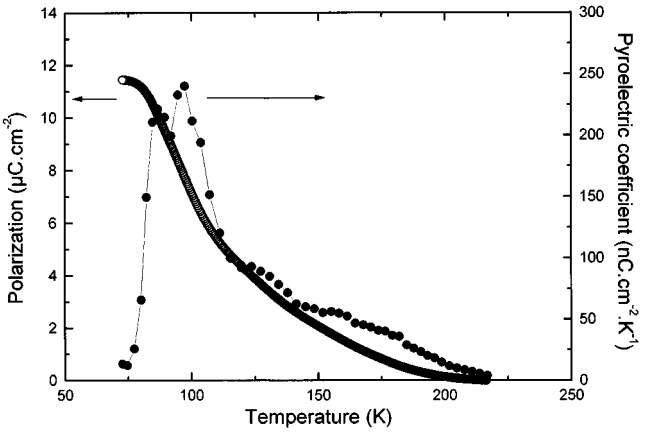

Fig. 8. Pyroelectric current (left scale) and polarization resulting from its integration (right scale) obtained from a Zero-Field Heating after Field Cooling experiment in BTZ40 [10].

preventing any first order Raman scattering. The appearance of Raman spectra at every temperature has been explained in these systems as resulting from the coupling of hard modes of the cubic centro-symmetric phase with the quasi-static polarization [3,4], according to the following expansion of the electronic polarizability tensor α:

$$\delta\alpha = \sum_i \frac{\partial\alpha}{\partial P_i} P_i + \sum_j \frac{\partial\alpha}{\partial Q_j} Q_j + \sum_{i,j} \frac{\partial^2\alpha}{\partial P_i \partial Q_j} P_i Q_j + ... \quad (1)$$

In this expression, P_i and Q_j refer to the quasi-static polarization and hard modes, respectively. The first term in the right hand side of equation (1) is at the origin of the so-called "central peak", and the second term corresponds to first order Raman scattering, which is forbidden by symmetry in the structures under consideration. The third term in equation (1) describes the second order Raman scattering which is responsible for the activation of the Raman lines. The integrated intensity of the spectra is obtained from the spatio-temporal auto-correlation function of the electronic polarizability (1), and is expressed as:

$$I(\omega) \propto \langle P(0,0)P(r,t)\rangle_{-q,\omega'} \langle Q(0,0)Q(r,t)\rangle_{q,\omega-\omega'} \quad (2)$$

where ω and ω' are the characteristic frequencies of the hard modes and of the quasi-static polarization respectively, with wavevectors $\pm q$, and the symbol $\langle\ \ \rangle_{q,\omega}$ denotes a space and time Fourier transformation. Below the freezing (Vogel-Fülcher) temperature, the auto-correlation function of the polarization in equation (2) is expected to saturate. This should be observed in the Raman scattered intensity as a plateau, as was already done in PLZT ceramics [3,9]. The BTZ40 relaxor obeys the same behaviour, as previously discussed and illustrated by Figure 7. The Raman freezing temperature of 120 K is in rather good agreement with the Vogel-Fulcher temperature of 145 ± 15 K determined from dielectric measurements. In addition, a field induced ferroelectric phase can be stabilized below the freezing temperature, when cooling the sample under a high enough electric field from high temperature. A Zero-Field Heating after Field Cooling (ZFH/FC) experiment should consequently result in a dielectric susceptibility anomaly and a depolarization current peak at the freezing temperature [9]. Both reflect the transition from the field-induced ferroelectric state to the ergodic relaxor phase. BTZ is thus expected to exhibit the same behaviour. The pyroelectric current obtained in a ZFH/FC run on BTZ40 is represented in Figure 8 [10]. It peaks at a temperature of 100 K, but extends up to above 175 K. This result is in good agreement with the above described behaviour, if we take into account the porous ceramic character of the BTZ40 sample.

It is now currently admitted [1] that polar nanodomains existing at high temperature are responsible for the relaxational properties of conventional relaxors such as PMN or PLZT. The correlation length of the polarization (which can be considered as related to the size of the nanodomains in an alternative scheme) increases on cooling, as already reported for PLZT [3,9] and observed in this work for BTZ from the variation of the Raman intensity with temperature (Fig. 7). Nevertheless, the intrinsic disorder prevailing in these systems (*e.g.*, negatively charged 1:1 domains with local stoichiometry Mg/Nb = 1 in PMN or charged point defects in PLZT) is a source of random fields which prevent any onset of long range ferroelectric order [11] and result in a plateau in the Raman intensity.

The present study of the evolution of the electrical and spectroscopic properties of BTZ with Zr composition provides an answer about the nature of the polar nanodomains in this system. It has been shown in the previous sections that a continuous change in the properties occurs on going from BT to the Zr-rich BTZ compositions. Because Zr ions are sources of random fields, the ferroelectric long range order prevailing in the BT rhombohedral phase is progressively broken, and only a polar nanoregion phase is stabilised at low temperature and zero field. This stable state is expected to be non-ergodic, in the same way as

in the other relaxors PMN [12] and PLZT [13]. It can be predicted from the phase diagram presented in Figure 2 that the local ordering in this state is also rhombohedral, because of the parent BT phase.

This assertion is supported by the evolution of the low temperature Raman spectra (Fig. 5). We pointed out in Section 4 that the interference effect detected at 125 cm^{-1} in the Zr-rich compounds could be considered as the signature of the local ordering around Zr ions. The corresponding line at 119 cm^{-1} in BTZ05 appears only at low temperature, *i.e.*, in the rhombohedral phase. The amplitude of these features strengthens on increasing the Zr substitution rate at 15 K from the rhombohedral phase to the frozen relaxor state. It can thus be inferred that local ordering in the relaxor phase is rhombohedral. Structural investigations similar to those performed in PMN [14] would be welcome in order to confirm this assertion.

Zirconium and titanium have the same valency, and these ions only slightly differ in their radii. The substitution of Ti by Zr is consequently not expected to give rise to strong random fields. This could be the reason why relaxor properties are obtained for rather high substitution rates ($>$ 27% Zr) in BTZ, when compared with the La-modification of PZT ceramics, for which relaxor properties appear above 7% La in 65/35 and 12% La in 40/60.

Finally, it should be kept in mind that, in relaxors, the temperature T_m of the dielectric susceptibility maximum has no specific physical meaning, from a dynamical point of view. It is just only located in the temperature range where a continuous change in the polarization distribution from polar nanoregions to a multidomain ("polar clusters") dynamic state takes place, as recently suggested by Shur *et al.* [15]. The most important transition temperature in these systems is the freezing point T_f, which corresponds to a drastic evolution in the dynamic properties and in a subsequent ergodicity breaking, as discussed above. This temperature has been already estimated in BTZ40 as $\sim$100$-$140 K from dielectric, Raman and pyroelectric current experiments. The accurate determination of these temperatures for the various compositions exhibiting relaxor properties in the BTZ system would suitably complete the phase diagram reported in Figure 2. Such determinations are currently under way.

The authors are indebted to "Région de Picardie" for its financial support.

References

1. L.E. Cross, Ferroelectrics **151**, 305 (1994).
2. J. Ravez, A. Simon, J. Korean Phys. Soc. **32**, S955 (1998).
3. M. El Marssi, R. Farhi, X. Dai, A. Morell, D. Viehland, J. Appl. Phys. **80**, 1079 (1996).
4. P. Di Antonio, B.E. Vugmeister, J. Toulouse, L.A. Boatner, Phys. Rev. B **47**, 5629 (1993).
5. M.E. Lines, A.M. Glass, *Principles and Applications of Ferroelectrics and Related Materials* (Clarendon Press, Oxford, 1977), p. 245, and references therein.
6. D. Hennings, A. Schnell, G. Simon, J. Amer. Ceram. Soc. **65**, 539 (1982).
7. A. Scalabrin, A.S. Chaves, D.S. Shim, S.P.S. Porto, Phys. Stat. Sol. B **79**, 731 (1977).
8. C.H. Perry, D.J. McCarthy, G. Rupprecht, Phys. Rev. **138**, A1537 (1965).
9. R. Farhi, M. El Marssi, J.-L. Dellis, J.-C. Picot, A. Morell, Ferroelectrics **176**, 99 (1996).
10. C. Broustera, R. von der Mühll (private communication).
11. M.D. Glinchuk, R. Farhi, J. Phys.-Cond. **8**, 6985 (1996).
12. A. Levstik, Z. Kutnjak, C. Filipic, R. Pirc, Phys. Rev. B **57**, 11204 (1998).
13. Z. Kutnjak, C. Filipic, R. Pirc, A. Levstik, R. Farhi, M. El Marssi, Phys. Rev. B **59**, 294 (1999).
14. N. de Mathan, E. Husson, G. Calvarin, J.-R. Gavarri, A.W. Hewat, A. Morell, J. Phys.-Cond. **3**, 8159 (1991).
15. V. Shur, V. Kuminov, G. Lomakin, S. Beloglazov, S. Slovikovski, A. Krumins, A. Sternberg, J. Korean Phys. Soc. **32**, S985 (1998).